Low-frequency electron dynamics in the near field of a Hall effect thruster

L. Albarède and S. Mazouffre[a)]
Laboratoire d'Aérothermique, 1C avenue de la Recherche Scientifique, 45071 Orléans, France

A. Bouchoule
GREMI, University of Orléans, 14 rue d'Issoudun B.P. 6744, 45067 Orléans, France

M. Dudeck
Laboratoire d'Aérothermique, 1C avenue de la Recherche Scientifique, 45071 Orléans, France

(Received 28 February 2006; accepted 9 May 2006; published online 14 June 2006)

Time-resolved electrostatic probe measurements were performed in the near field of a SPT100-ML Hall effect thruster in order to investigate electron properties changes on a microsecond time scale. Such measurements allow one to monitor the electron temperature T_e, the electron density n_e, as well as the plasma potential V_p during a time period that corresponds to one cycle of a breathing-type plasma oscillation with $f \approx 15-30$ kHz. Although $T_e(t)$ stays constant in time, $n_e(t)$ and $V_p(t)$ oscillate with the discharge current waveform frequency. The observed time delay between n_e and anode discharge current (Id_a) waveforms, which is of approximately 7 μs, is linked to the ion transit time from the ionization layer to the probed near-field region. The same time gap is measured between $V_p(t)$ and $Id_a(t)$, however $V_p(t)$ and $n_e(t)$ are in phase opposition. The electron density reaches its highest value at the very moment ions are ejected out of the thruster discharge chamber, which also corresponds to the instant the cathode potential is the most negative. Such a behavior images the need for ion beam neutralization. Further, it is shown that there is a strong correlation between the electron dynamics and the presence of high frequency (HF) plasma oscillations in the megahertz range: HF fluctuations are the strongest when n_e is the highest.
 [DOI: 10.1063/1.2209628]

I. INTRODUCTION

Electric propulsion is nowadays a well-established concept for space applications.[1,2] Among all proposed electric propulsive devices such as arcjet, magnetoplasma dynamic thruster, gridded ion engine and Hall effect thruster (HET), the latter is currently recognized as an attractive propulsion means for long duration missions and for maneuvers that require a large change of velocity. Hall effect thrusters, also called stationary plasma thrusters or closed electron drift thrusters, are advanced propulsion devices that use an electric discharge to ionize and accelerate a propellant gas.[3,4] Due to interesting features in terms of propellant ejection speed, efficiency, flexibility and lifetime, HET are now employed for missions like geostationary satellite orbit correction and station keeping. The use of high power Hall thrusters for orbit transfer maneuvers would also offer significant benefits in terms of launch mass, payload mass and operational life. Further, HETs appear as good candidates to be employed as the primary propulsion engine for space probes during interplanetary trips, as demonstrated by the successful SMART-1 mission of the European Space Agency.[5]

The basic physics of a HET implies a magnetic barrier in a low pressure dc discharge generated between an external hollow cathode and an anode.[3,6,7] The anode, which also serves as gas injector, is located at the upstream end of a coaxial annular dielectric channel that confines the discharge. Xenon is generally used as a propellant gas for its specific properties in terms of high atomic mass and low ionization energy. A set of solenoids provides a radially directed magnetic field **B** of which the strength is maximum in the vicinity of the channel exhaust. The magnetic field is chosen strong enough to trap electrons around Larmor orbits, but weak enough not to disturb ion trajectories. The electric potential drop between anode and cathode is mostly concentrated in the final section of the channel owing to the low electron axial mobility in this restricted area. The corresponding induced local axial electric field **E** has two main effects. First it drives a high electron azimuthal drift—the so-called Hall current—that is responsible for the efficient ionization of the supplied gas. Second, it accelerates the created ions, which form the thruster plasma plume. The ion beam is neutralized by a fraction of electrons emitted from the hollow cathode. A HET similar to the one used onboard the SMART-1 lunar probe, when operating approximately at 1.5 kW, ejects ions at 20 km s^{-1} and generates 80 mN of thrust with an overall efficiency of approximately 50%.[4]

The magnetized plasma of a Hall effect thruster displays numerous type of oscillations, which encompass many kind of physical phenomena each of them with its own length and time scales.[6,8] Discharge and plasma instabilities, of which the spectrum stretches from the kilohertz to the gigahertz frequency domain, play a major role in ionization, particle diffusion and acceleration processes. When they become unstable plasma oscillations may, however, be at the origin of a decrease in overall thruster performances. Unstable oscillations can damage the electric power supply and they can

[a)]Author to whom correspondence should be addressed. Electronic mail: stephane.mazouffre@cnrs-orleans.fr

even lead to the extinction of the discharge.[8] Physical mechanisms at the origin of low frequency plasma oscillations in the kilohertz range, the so-called breathing-type oscillations are nowadays well understood [8] and well described by means of hybrid HET models.[8,9] Moreover, the impact of such plasma oscillations on the ion flow and the plume properties is well documented.[10,4] On the contrary, and despite many years of in-depth research, high-frequency discharge instabilities linked to electron transport are not yet fully grasped, which limits the design and development of high power Hall thruster and prevents numerical simulations to be used as predictive tools.

Low-frequency oscillations in the kilohertz range dominate the power spectrum of discharge and plasma instabilities in Hall effect thrusters.[4,9,11] These oscillations originate in a periodic depletion and replenishment of the neutrals near the exit of the thruster.[8,9] In that area, the strong magnetic field lowers the electron conductivity, which in turn leads to an increase of the electric field required to maintain current continuity. Therefore, the ionization process is enhanced, leading to a depletion of the neutral density. Then the ionization front moves backward in the channel to an area where the ionization process is not as efficient, thus allowing the neutral flow to move forward again. This "prey-predator" cycle will then restart causing an oscillation whose frequency falls in the 15–30 kHz range. In literature, this specific type of oscillations is often refer to as "breathing oscillations."[9]

In the past few years, the ion beam transient behavior over the time scale of breathing oscillations has been extensively characterized by means of various diagnostic tools like Charged Coupled Device (CCD) imaging, retarding potential analyzer, and emission spectroscopy.[10,12,13] However, to the best of our knowledge, nobody investigated the temporal behavior of electron properties in the thruster near field and in the plasma plume. In other words, only time-averaged quantities were measured.[14,15] In the present contribution, we examine variations of electron temperature T_e and density n_e, as well as plasma potential V_p during one low-frequency current oscillation cycle that correspond to approximately 40 μs. Time-resolved electric probe measurements were carried out at the microsecond time scale in the near field of a SPT100-ML thruster exhaust. The study of the electron dynamics in this specific area is of great interest in view of its peculiarities. It is a region of high magnetic field through which ions are ejected from the thruster channel and where the neutralization of the ion beam starts. Consequently, this area corresponds to the region of interaction between the thruster plasma and the electron stream that originates from the hollow cathode. In addition to probe data analysis, the evolution through time of electron properties and plasma potential is compared with changes in thruster parameters like discharge current and cathode potential. Finally, we investigate possible link between behavior of electron properties at breathing oscillation time scale and plasma instabilities observed in the megahertz frequency domain.

II. TIME-RESOLVED ELECTRIC PROBE MEASUREMENTS

A. Setup, instrument, and method

All experiments described in the paper were carried out with a laboratory version of a SPT100 Hall effect thruster, so-called SPT100-ML, equipped with $BN-SiO_2$ discharge chamber walls in the PIVOINE ground-test facility.[16] In the course of the measurement campaign, the thruster was operated under standard conditions: 300 V applied voltage, 5 mg s^{-1} xenon gas flow rate through the anode and 2×10^{-5} mbar background pressure. The mean discharge current was approximately 4.4 A and the thrust reached 82 mN.

The discharge current oscillations were directly monitored on the thruster power circuit by means of a 50 MHz bandwidth current probe (Lecroy AP015). The current could be measured either on the cathode wire (Id_c) or on the anode wire (Id_a). The cathode and anode potential with respect to ground (V_c, V_a) were recorded by means of a 15 MHz bandwidth differential probe pair. A dedicated electric single probe has been built up to especially monitor electronic measurable quantities in the near field of the thruster. The electric probe is based on a coaxial cable architecture. The core of the probe is a tungsten wire able to endure high temperature. It is 100 μm in diameter and the part in contact with the plasma is solely 2 mm in length. The nonactive part of the core is inserted into a small alumina tube that acts as an inner dielectric insulator. The outer conductor, i.e., the screen, is made of stainless steel. Finally the outer insulator is in alumina. The probe impedance is close to 50 Ω. The probe is connected to a 50 Ω SMA cable. Vacuum feed-through is achieved by 50 Ω wide band coaxial connectors. The low-impedance coaxial design of the probe warrants a low noise level and no distortion of signals even at high frequency. Such probes are well suited to capture broadband signal induced by plasma oscillations.[17] A voltage source allows variation of the probe potential with respect to the plasma in order to determine the current-voltage characteristic. The current delivered by the probe is measured over a 1 kΩ resistor. It is also possible to measure the floating probe potential when connecting the latter to ground through a very high resistance. All signals are recorded by means of a 1 GHz bandwidth fast sampling oscilloscope. The discharge current signal is used as a trigger to synchronize waveform acquisition. The probe is mounted horizontally in the half-plane that contains the cathode. It is located 1 cm in front of the thruster exit plane near the plasma plume boundary layer, see Fig. 1. No change in discharge properties were observed when inserting the probe into the plasma medium as in the work of Staack and co-workers.[18]

The examination of the electron dynamics over the time scale of breathing oscillations, i.e., with a time resolution below 1 μs, necessitate to collect a vast dataset in the form of time-resolved probe characteristics. Several measurement series, which as we will see correspond to different probe potential, are performed one after each others with an overall acquisition duration that exceeds several minutes. The state of the thruster discharge must naturally be identical for every single measurement in order to obtain a coherent dataset.[19]

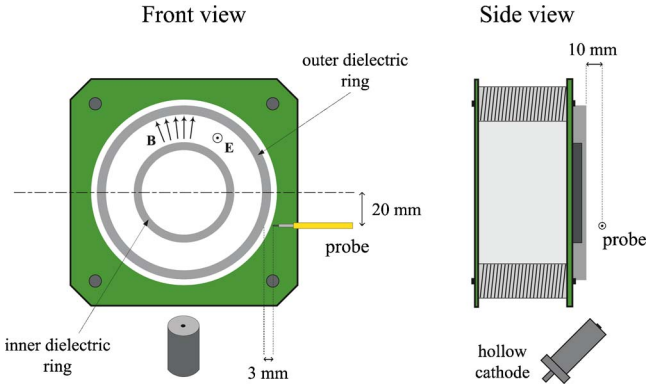

FIG. 1. Schematic drawing of a Hall effect thruster and location of the Langmuir probe.

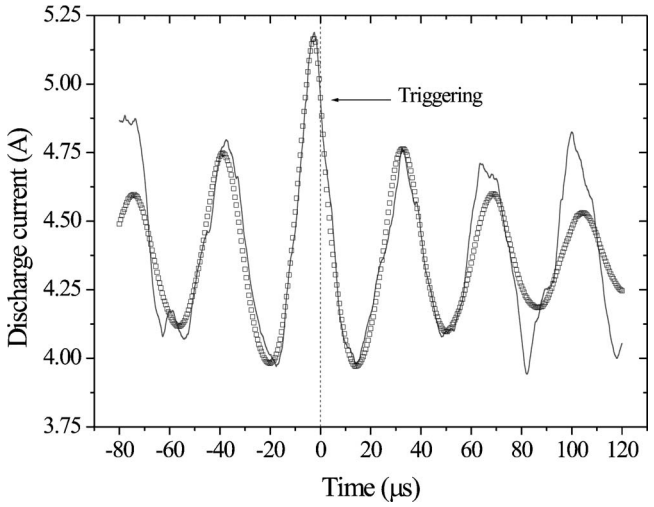

FIG. 2. Hall effect thruster anode discharge current (Id_a) waveform averaged over 128 cycles (square). Single shot measurement of Id_a (line). The trigger level is set to 4.95 A and data acquisition starts at $t=0$ μs.

To a large extent, the HET plasma state can be characterized by the oscillation level of the discharge current for a given discharge voltage and xenon mass flow rate. However, low-frequency plasma oscillations in the 15–30 kHz range are nonstationary meaning that even at fixed thruster working parameters the frequency and the amplitude of such oscillations vary in time.[11] Therefore, one must find a way to select identical events, which, in addition, must correspond to the average behavior of the plasma.

According to previous criteria, data acquisition settings are the proper ones when any random single shot measurement of the discharge current waveform matches the mean discharge current waveform. Obviously, if the oscilloscope trigger level is set either too high or too low, the corresponding events do not image at all the mean state of the thruster discharge. The electric probe signal acquisition method is the following. The measurement time period is set to 100 μs in order to cover several current oscillation periods. Under standard operating conditions, the mean value of the SPT100-ML anode discharge current is 4.4 A. The oscilloscope trigger level is set to a value 10% higher than the mean value to only select plasma states close to the mean state. The recorded electric probe signal is the ensemble average of 128 samples. In Fig. 2 the averaged current profile obtained over the measurement sequence is superimposed to a current waveform snapshot. The two profiles overlap during 100 μs indicating a proper choice of triggering procedure.

Using the aforementioned acquisition method, the electric probe response is recorded as a function of time for a given polarization potential. In order to be able to reconstruct the current-voltage ($I-V$) probe characteristic from which electron properties are extracted, the polarization potential must be varied from positive to negative values. The probe is polarized from −30 to +61 V with 1 V steps. In Fig. 3, the current collected by the probe is displayed as a function of time for several polarization voltage. The mean anode discharge current is superimposed to the probe response. The ensemble of recorded time-resolved probe response allows to build probe characteristic and to calculate the electron properties $T_e(t)$, $n_e(t)$ as well as floating potential $V_f(t)$ and plasma potential $V_p(t)$ at a precise time.

B. Analysis of probe characteristics

An example of reconstructed current-voltage probe characteristic is shown in Fig. 4. This curve corresponds to the probe response at $t=3.49$ μs. The $I-V$ probe characteristics obtained at a given time were analyzed using the classical theory of electric probe.[20–22] Under our condition, the electron mean free path for collisions with ions or electrons is much longer than sheath thickness, which is in the order of the Debye length $\lambda_D \approx 200$ μm, meaning that the plasma sheath surrounding the probe is collisionless. The electron mean free path is greater than the probe diameter that warrants no disturbance of the plasma flow. In the region of measurement, the magnetic field magnitude is approximately 100 G and the electron Larmor radius is approximately 1 mm, i.e., larger than the probe tip diameter. In our case, the probe orientation with respect to **B** can lead to a decrease in the collected electron current. However, the relatively large Larmor radius can counterbalance the effect of the probe orientation. The theory of Langmuir probes becomes com-

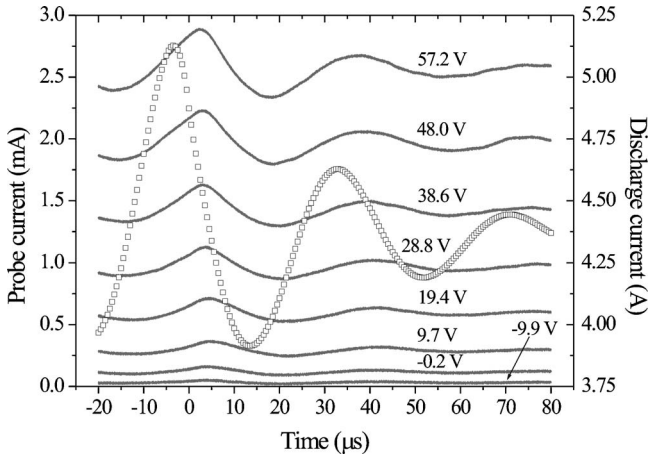

FIG. 3. Current collected by the electric probe as a function of time for several polarization voltage (line). Also shown is the averaged thruster discharge current with $f=27.5$ kHz (square).

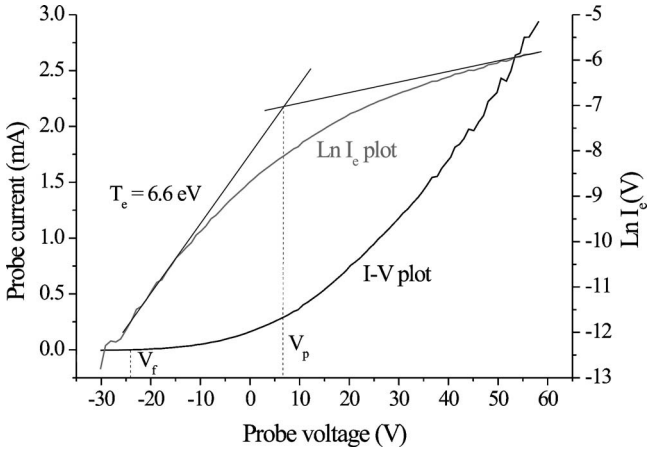

FIG. 4. Probe characteristic at $t=3.49$ μs. Also shown is the plot $\ln(I_e)$ as a function of the probe voltage. V_f is the probe floating potential, V_p is the plasma potential, and T_e is the electron temperature.

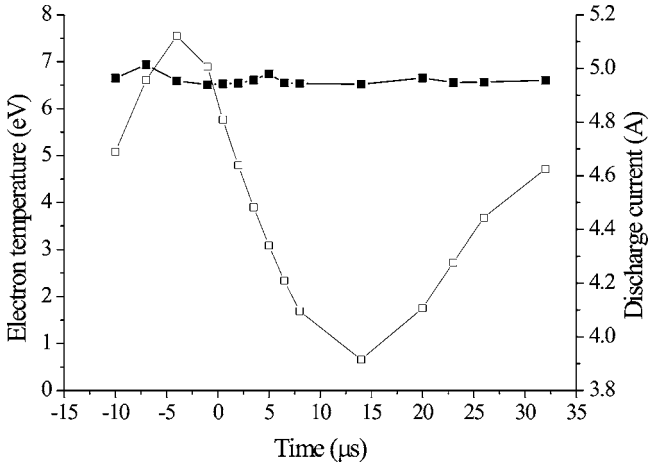

FIG. 5. Development of the electron temperature over one low-frequency oscillation cycle (filled square). The anode discharge current as a function of time is also shown (open square).

plex when the plasma is magnetized, see, e.g., Refs. 20 and 22. The collection area of the probe is modified and a correction factor must be determined. This task is however not straightforward when the magnetic field topology is complicated. Moreover, other effects like cross-field currents, magnetic sheath, and viscosity must be taken into account. As no quantitative theory is as yet available we decided not to correct the probe $I-V$ characteristics. Moreover, we are mostly interested in the evolution of n_e and T_e in time and not in determining absolute numbers.

To extract the electron temperature T_e and density n_e from the probe $I-V$ curve, the electron energy distribution function (EEDF) was assumed to be Maxwellian. Indeed, electric probe measurement at the exhaust of a SPT50 HET revealed that, though non-Maxwellian, the EEDF is largely dominated by a group of relatively cold electrons that forms an equilibrium population.[15] For an extensive discussion about single probe measurement analysis, the reader can refer to Ref. 22. The floating potential V_f is the potential for which ion and electron current are equal. If the EEDF is Maxwellian, the electron current I_e exhibits exponential behavior for repulsive potentials and thus $\ln(I_e)$ is a linear function. The electron temperature is obtained from the slope of the linear part of the semilog plot of I_e after subtracting the ion saturation current. The plasma potential V_p corresponds to the intersection between the linear part and the tangent of the electronic branch in saturation regime. Figure 4 displays the $\ln(I_e)$ curve obtained from the $I-V$ plot at $t=3.49$ μs as well as V_f, V_p, and T_e. The experimental error in T_e is estimated to be ± 1 eV. The measurement uncertainty of V_p is approximately ± 5 V. The electron density n_e is found from the electron saturation current $I_{e,\mathrm{sat}}$:

$$n_e = \frac{I_{e,\mathrm{sat}}}{eS\sqrt{\frac{k_B T_e}{2\pi m_e}}}, \tag{1}$$

where e is the elementary charge, S is the probe area, k_B is the Boltzmann constant, and m_e is the electron mass. The $I-V$ probe characteristics displayed in Fig. 4 does not exhibit a knee which is the usual signature for the electron saturation regime. The observed trend is a direct consequence of the existence of a relatively strong magnetic field in the measurement region. To draw a tangential line to the saturation part of the $\ln(Ie)$ curve is rather tricky, hence a large measurement uncertainty for V_p. Under our conditions, the use of the second derivate of the discrete $I-V$ probe characteristic to estimate the EEDF was not possible: $I-V$ plots are not smooth enough and curve fitting as well as interpolation generate results with a great inaccuracy.

III. ELECTRON PROPERTIES AT "BREATHING OSCILLATION" TIME SCALE

The development of the electron temperature T_e as a function of time is shown in Fig. 5 during a time period that corresponds to one cycle of the thruster discharge current. The electron temperature remains constant and there is no relation between current oscillation and temperature. In the regime of moderate input power and low level of current oscillation, the mean electron temperature is approximately 6.5 eV in the near field of the SPT100 thruster, in agreement with values reported for similar HET.[14,23] The constant temperature of the main electron group, which dominates the EEDF, means that in the near field no energy exchange process can modify in a significant way the electron temperature at the microsecond time scale.

The Langmuir probe is located 1 cm behind the thruster channel exhaust, see Fig. 1, a region where the electric field is weak.[24] Thus, in the probed area electrons cannot gain much kinetic energy by way of the local electric field. In like manner, there is no energy loss channel for electrons in the plasma plume near field as energy transfer owing to collision with heavy particles is not favored. First, the xenon atom density is relatively low that leads to a frequency for e-atom impact of approximately 10^6 s^{-1}. Second, exchange of energy in a collision depends upon the ratio of xenon atom mass to electron mass. As a consequence, the relaxation time for electron energy transfer by impact lies in the ms range, which is much greater than the characteristic time scale of

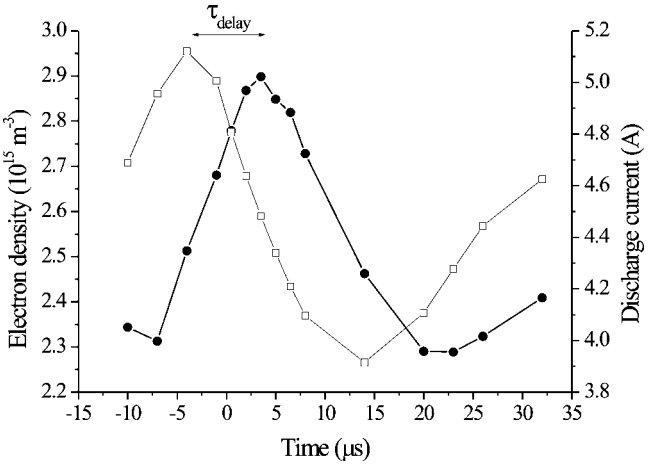

FIG. 6. Development of the electron density over one low-frequency oscillation cycle (circle). The anode current as a function of time is also shown (square). The time delay τ_{delay} between the two waveforms is approximately 7 μs.

breathing oscillations. As we will see in Sec. V HF oscillations in the megahertz domain are observed during specific periods of time.[17,25] HF oscillations could participate in the overall electron energy balance, hence influencing the electron temperature T_e. However a microsecond time resolution prevents from observing any direct effect of HF oscillations on the temporal behavior of T_e. Only a mean value is accessible.

Unlike T_e, the electron density does oscillate in time as can be seen in Fig. 6. The n_e oscillation frequency is approximately 28 kHz as the anode current oscillation frequency. The plasma potential oscillates at a frequency of approximately 30 kHz, see Fig. 7. The two quantities oscillate at the frequency of $Id_a(t)$, however, they are in phase opposition. Moreover, they both are phase shifted with respect to the anode discharge current. As can be observed in Fig. 6, the time delay τ_{n_e} between $n_e(t)$ and $Id_a(t)$ is 7 μs. Looking at data in Fig. 3, one finds $\tau_{n_e} \approx 6$ μs using the signal measured at high probe voltage when solely electrons are collected.

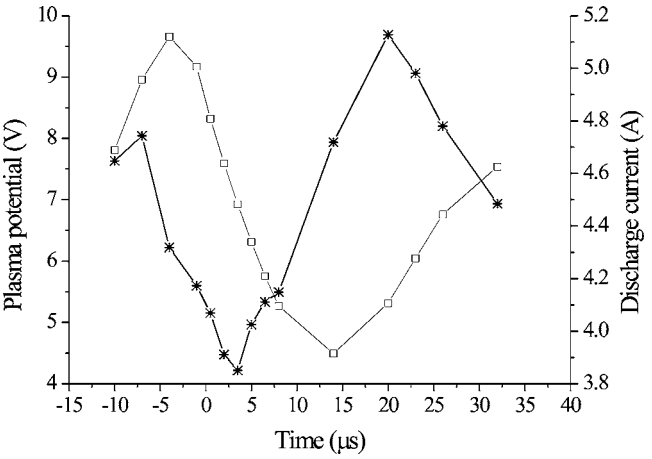

FIG. 7. Development of the plasma potential over one low-frequency oscillation cycle (star). The anode current as a function of time is also shown (square). V_p is the lowest when n_e is the greatest, see Fig. 6.

The observed time delay is certainly connected with the ion time of flight from the ionization layer to the probed zone. Indeed, the anode discharge current images the creation of ions inside the channel, and the increase of electron density recorded by the electrostatic probe reveals the flow of ions. The measured time delay therefore corresponds to the time it takes ions to travel through the acceleration layer. Note that for a Hall effect thruster the ion time of flight depends upon both the applied voltage and the magnetic field map.[19]

As can be seen in Fig. 6, the electron density reaches a maximum during a decrease stage of the anode discharge current, in other words when the slope of the current waveform is negative. As already mentioned, the plasma potential is the lowest at the time n_e is the highest, see Fig. 7. It obviously results from the fact that the higher the amount of electrons the more negative the local plasma potential. Time-resolved optical measurements indicated that ion bunches are indeed created at the breathing instability frequency.[10,12] Time-resolved CCD imaging of the plasma plume performed after an ultrafast discharge current ignition have shown that ejected ions propagate in the thruster near field when the condition $dId_a(t)/dt < 0$ is fulfilled.[10,26] Moreover, the ion propagation speed was measured in the channel exhaust vicinity by means of laser spectroscopy[24]: the mean ion speed in the zone of interest is in the order of 7 km/s (SPT100-ML in standard operating conditions). The distance between the ion creation zone and the probe being 25 mm, it takes approximately 4 μs for ions to reach the probe. It now becomes obvious that electron density and plasma potential oscillations in the thruster near field image the ion beam neutralization process.

IV. TEMPORAL EVOLUTION OF THRUSTER DISCHARGE PARAMETERS

The behavior of the SPT100-ML Hall effect thruster discharge parameters, i.e., currents and voltages, have been monitored as a function of time in standard operating conditions. Corresponding plots are shown in Fig. 8 for a time period of 100 μs. Naturally, the behavior of discharge parameters is strongly correlated with the electron property evolution in time, as we will see in the remainder of this section.

In the upper graph of Fig. 8, oscillations of Id_a and Id_c are displayed as well as the difference between the two quantities. The two currents are almost in phase, however, a few μs after the peak, the decay of Id_c is less pronounced. At this very moment n_e reaches its maximum value, see Fig. 6. The difference in shape between Id_a and Id_c waveforms occurs exactly when ions are ejected out of the thruster channel. The gap between cathode and anode discharge currents correspond to the amount of electric charges flowing out of the discharge chamber Q_{out} for a given period of time: $[Id_c(t) - Id_a(t)] \times \Delta t = Q_{\text{out}}$. Naturally, when the left-hand side of the previous equation is integrated over a long period of time, one finds $Q_{\text{out}} = 0$. As can be seen in Fig. 8, $Q_{\text{out}} > 0$ during a trough of Id_a curve, i.e., at the beginning of a new ion creation stage inside the channel, or in other words at the moment ions flow outside the channel. Q_{out} therefore mostly

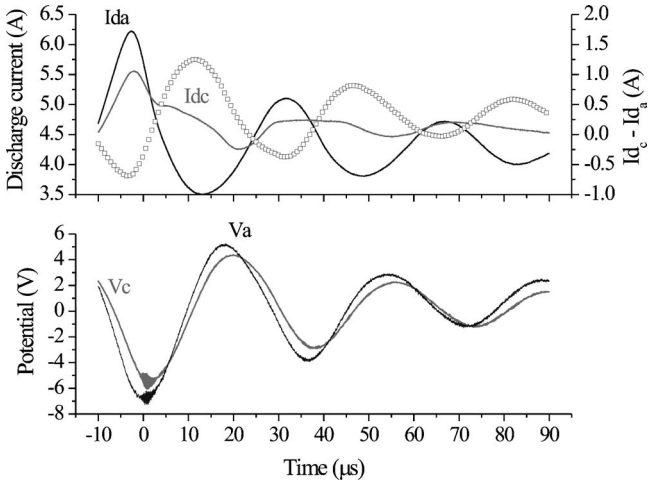

FIG. 8. Mean value of the SPT100-ML thruster anode and cathode discharge current as a function of time (top). Also shown in this plot in the difference between the two quantities (square). Evolution in time of both the anode and the cathode potential after subtraction of their mean value (bottom): $\bar{V}_a$=276.0 V and $\bar{V}_c$=−21.5 V. All curves result from the ensemble average of 128 waveforms.

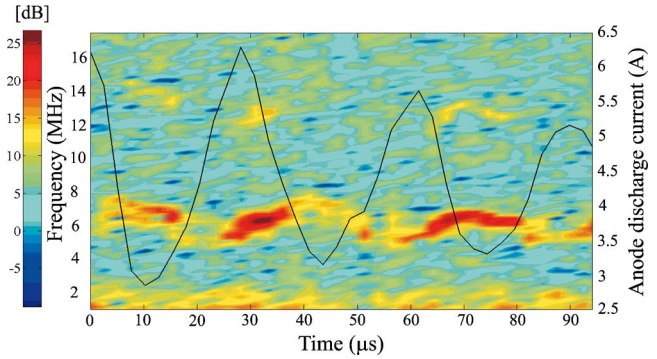

FIG. 9. (Color online) High frequency part of the time-dependent power spectrum of the thruster cathode potential V_c. The superimposed solid line represents the evolution in time of the anode discharge current Id_a.

corresponds to the quantity of charges necessary to neutralize the ion beam.

In the lower graph of Fig. 8, cathode and anode potential waveform are slightly shifted in time, with a delay approximately 2.5 μs. Note that the cathode potential, with respect to ground, is negative. Also shown in Fig. 8, is the fact that $Id_a(t)$ and $V_c(t)$ exhibit a time shift of approximately 5 μs. Moreover, V_c is the most negative when Id_c departs from its expected behavior, as previously discussed. Observed trends can be explained as follows. In the near field of a Hall effect thruster, the electron density n_e reaches a maximum value at the moment ions exit the channel. The time delay between Id_a and n_e, which is linked to the ion time of flight through the potential fall, depends upon the exact location of the electrostatic probe. Electrons, that are needed to neutralize the ion beam, are produced by the hollow cathode. As soon as ions are ejected out of the thruster channel, the cathode must respond to the inrush current. It produces a burst of electrons, hence a more negative potential, which in turn allows to easily repel electrons toward the plasma plume. A last remark can be made. As can be seen in Fig. 7, cathode waveform $V_c(t)$ and plasma potential waveform $V_p(t)$ are in phase. The observed phase-locking property suggests that potential changes occur everywhere at the same time being then an overall plasma phenomenon.

V. ELECTRON DYNAMICS VERSUS HF OSCILLATIONS

A last point is worth discussing. HF Hall effect thruster plasma oscillations in the megahertz domain have again attracted attention over the past years in view of their possible implications in the phenomenon of anomalous electron transport across the thruster magnetic barrier. Numerous works devoted to both measurement and analysis of such high frequency signals are nowadays reported in literature, see, e.g., Refs. 11, 17, and 27. Nevertheless, there is not so far any direct proof for a link between electron motion and the existence of HF plasma oscillations.

The high-frequency part of the time-dependent power spectrum of the cathode potential V_c is displayed in Fig. 9. The power spectrum was obtained using short-time Fourier transform for simplicity's sake, although such a tool is not perfectly appropriated to analyze nonstationary signal like Hall effect thruster plasma oscillations.[11] The existence of HF signals with $f \approx 6$ MHz is clearly visible in Fig. 9. Note that HF oscillations are also observed when analyzing $Id_a(t)$ and $Id_c(t)$ current waveforms[11,17] even though they appear to be weaker in that case. On the contrary, HF components have never been detected when monitoring oscillations of the anode potential. It may indicate that HF plasma oscillations are solely produced in the region where both the magnetic field is high and the particle density is low, i.e., in a region where anomalous electron transport dominates. As can be seen in Fig. 9, the 6 MHz oscillations appear in the form of bursts: the amplitude of the HF oscillations is maximum during a decrease stage of the anode discharge current. For a detailed review about the dynamics of high frequency oscillations in a Hall thruster the inclined reader can refer to.[11] What is interesting here is the following fact: the highest HF signal amplitude coincides with a maximum of the electron density in the near field, see Fig. 6. This mere property suggests a link between high frequency plasma oscillations and electron dynamics in the outer plasma. As soon as neutralization process begins in the thruster near field a large number of electrons must travel through the magnetic field to maintain ionization inside the channel. High frequency plasma oscillations could then be a kind a signature for anomalous electron transport across the magnetic field. However, even if outcomes of this work reveal a HF signals-electron properties relation, the question about the origin of the high frequency plasma fluctuations is still opened.

VI. CONCLUSION

Electrostatic probe measurements have been performed in the near field of a SPT100-ML Hall effect thruster with a microsecond time resolution. Such a diagnostic tool allowed to determine electron properties changes over a time scale

that corresponds to breathing-type plasma oscillation. $T_e(t)$ stays constant in time, meaning that the electron energy balance is not disturbed, whereas $n_e(t)$ and $V_p(t)$ oscillate with the discharge current waveform frequency ($f \approx 30$ kHz). It is shown that the observed behavior images the ion beam neutralization process. Moreover, this work brings to light a link between high frequency plasma oscillations in the megahertz domain and electron dynamics.

This work can be seen as a first step. Indeed, in order to confirm our results and to get more precise insights into electron dynamics behind the channel exhaust, measurements should not only be time-resolved but also spatially-resolved. A set of Langmuir probes placed at various locations could be employed to observe the evolution of electron properties in time as well as in space. In such a way it may for instance be possible to distinguish between transport phenomena from the cathode to the channel entrance and from the cathode to the downstream plasma plume.

ACKNOWLEDGMENTS

This work is carried out in the frame of the research group CNRS/CNES/Snecma/Universités 2759 "*Propulsion Spatiale à Plasma*." It is financially supported by the French Space Agency (CNES) and the Région Centre. P. Lasgorceix and C. Legentil are gratefully acknowledged for their skillful assistance.

[1] G. Saccoccia, J. Gonzalez del Amo, and D. Estublier, *ESA bulletin* Vol. 101 (ESA Publications Division, Noordwijk, The Netherlands, 2000).
[2] R. H. Frisbee, J. Propul. Power **19**, 1129 (2003).
[3] V. V. Zhurin, H. R. Kaufman, and R. S. Robinson, Plasma Sources Sci. Technol. **8**, R1 (1999).
[4] N. Gascon, M. Dudeck, and S. Barral, Phys. Plasmas **10**, 4123 (2003).
[5] C. R. Koppel, F. Marchandise, M. Prioul, D. Estublier, and F. Darnon, *Proceedings of the 41th Joint Propulsion Conference and Exhibits*, Tucson, AZ (American Institute of Aeronautics and Astronautics, Reston, VA, 2005), AIAA Paper No. 05-3671 (2005).
[6] A. I. Morozov and V. V. Savelyev, in *Reviews of Plasma Physics*, edited by B. B. Kadomtsev and V. D. Shafranov (Kluwer Academic, Plenum Publisher, New York, 2000), pp. 203–391, Vol. 21.
[7] V. Kim, J. Propul. Power **14**, 736 (1998).
[8] E. Y. Choueri, Phys. Plasmas **8**, 1411 (2001).
[9] J. P. Boeuf and L. Garrigues, J. Appl. Phys. **84**, 3541 (1998).
[10] V. Vial, S. Mazouffre, M. Prioul, D. Pagnon, and A. Bouchoule, IEEE Trans. Plasma Sci. **33**, 524 (2005).
[11] J. Kurzyna, S. Mazouffre, A. Lazurenko, L. Albarède, G. Bonhomme, K. Makowski, M. Dudeck, and Z. Peradzyński, Phys. Plasmas **12**, 123506 (2005).
[12] A. Bouchoule *et al.*, Plasma Sources Sci. Technol. **10**, 364 (2001).
[13] D. Pagnon, F. Darnon, S. Roche, S. Béchu, L. Magne, A. Bouchoule, M. Touzeau, and P. Lasgorceix, *Proceedings of the 35th Joint Propulsion Conference and Exhibits*, Los Angeles, CA (American Institute of Aeronautics and Astronautics, Reston, VA, 1999), AIAA Paper No. 99-2428.
[14] Y. Raitses, D. Staack, M. Keidar, and H. J. Fisch, Phys. Plasmas **12**, 057104 (2005).
[15] V. Yu. Fedotov, A. A. Ivanov, G. Guerrini, A. N. Vesselovzorov, and M. Bacal, Phys. Plasmas **6**, 4360 (1999).
[16] A. Bouchoule, A. Cadiou, A. Héron, M. Dudeck, and M. Lyszyk, Contrib. Plasma Phys. **41**, 573 (2001).
[17] A. Lazurenko, V. Vial, M. Prioul, and A. Bouchoule, Phys. Plasmas **12**, 013501 (2005).
[18] D. Staack, Y. Raitses, and N. J. Fisch, Rev. Sci. Instrum. **75**, 393 (2004).
[19] F. Darnon, Ph.D. thesis, University of Orléans, France, 1999 (in French).
[20] F. F. Chen, in *Plasma Diagnostic Techniques*, edited by R. H. Huddlestone and S. L. Leonard (Academic, New York, 1965), p. 113.
[21] *Plasma Diagnostics*, edited by A. A. Ovsyannikov and M. F. Zhukov (Cambridge International Science Publishing, Cambridge, UK, 2000), p. 219.
[22] V. I. Demidov, S. V. Ratynskaia, and K. Rypdal, Rev. Sci. Instrum. **73**, 3409 (2002).
[23] V. Kim *et al.*, *Proceedings of the 29th International Electric Propulsion Conference*, Princeton University, NJ (Electric Rocket Propulsion Society, Cleveland, OH, 2005), IEPC Paper No. 05-04.
[24] N. Dorval, J. Bonnet, J. P. Marque, E. Rosencher, S. Chable, F. Rogier, and P. Lasgorceix, J. Appl. Phys. **91**, 4811 (2002).
[25] J. C. Adam A. Héron, and G. Laval, Phys. Plasmas **11**, 295 (2004).
[26] L. Albarède, Ph.D. thesis, University of Orléans, France, 2004 (in French).
[27] A. A. Litvak, Y. Raitses, and N. J. Fisch, Phys. Plasmas **11**, 1701 (2004).